# A Method to Estimate Vertically Integrated Amounts of Cloud Ice and Liquid and Mean Rain Rate in Stratiform Precipitation from Radar and Auxiliary Data

SERGEY Y. MATROSOV

*Cooperative Institute for Research in Environmental Sciences, University of Colorado, and NOAA/Earth System Research Laboratory, Boulder, Colorado*

(Manuscript received 27 August 2008, in final form 26 January 2009)

ABSTRACT

A method to retrieve total vertical amounts of cloud liquid and ice in stratiform precipitating systems is described. The retrievals use measurements from the vertically pointing $K_a$- and W-band cloud radars operated by the U.S. Department of Energy Atmospheric Radiation Measurement (ARM) Program and auxiliary measurements from a scanning National Weather Service radar and a ground-based disdrometer. Separation between the cloud liquid and rain is based on estimations of the total attenuation of millimeter-wavelength radar signals in the liquid hydrometeor layer. Disdrometer measurements are used for the retrieval constraints. Because the liquid phase hydrometeor retrievals use only differential measurements, they are immune to the absolute radar calibration uncertainties. Estimates of the ice cloud phase are performed using empirical relations between absolute radar reflectivity and ice water content. Data from the nearby scanning weather-service radar, which operates at a lower frequency, are used to correct cloud radar measurements observed above the freezing level for attenuation caused by the layers of liquid and melting hydrometeors and also by wet radomes of cloud radars. Polarimetric and vertical Doppler measurements from ARM cloud radars provide a distinct separation between regions of liquid and ice phases, and therefore the corresponding retrievals are performed in each region separately. The applicability of the suggested method is illustrated for a stratiform precipitation event observed at the ARM Southern Great Plains facility. Expected uncertainties for retrievals of cloud liquid water path are estimated at about 200–250 g $m^{-2}$ for typical rainfall rates observed in stratiform systems (~3–4 mm $h^{-1}$). These uncertainties increase as rainfall rate increases. The ice water path retrieval uncertainties can be as high as a factor of 2.

## 1. Introduction

A comprehensive characterization of hydrometeors in the vertical atmospheric column is one of the important objectives of the U.S. Department of Energy Atmospheric Radiation Measurement Program (ARM; Ackerman and Stokes 2003). Until recently the main interest of the ARM-based hydrometeor characterization and remote sensing activities was primarily focused on the development and application of the methods to retrieve radiatively important microphysical parameters of nonprecipitating clouds. A number of techniques have been suggested for estimating layer mean values and vertical profiles of liquid and ice cloud properties with the use of the ARM ground-based instrumentation. Intercomparisons of many ARM nonprecipitating cloud retrieval techniques are given in recent review articles by Comstock et al. (2007) and Turner et al. (2007).

Retrievals of parameters of precipitating clouds are generally more challenging. This is especially true for the ARM Climate Research Facilities (ACRF) where most cloud sensing instruments (including millimeter-wavelength radars) were primarily designed for measuring properties of nonprecipitating clouds. It has been shown, however, that cloud radars operating with a vertical beam at $K_a$ band (wavelength $\lambda \sim 8$ mm) or W band ($\lambda \sim 3$ mm) can be used for rainfall retrievals when attenuation-based radar approaches are applied (e.g., Matrosov 2005; 2007; Matrosov et al. 2008a). These approaches use attenuation effects, which often dominate the vertical gradient of reflectivity observed in rain at millimeter wavelengths, as a source of information for estimating rainfall rate and were applied to the

*Corresponding author address:* Sergey Y. Matrosov, R/PSD2, 325 Broadway, Boulder, CO 80305.
E-mail: sergey.matrosov@noaa.gov

DOI: 10.1175/2009JAMC2106.1

measurements of ARM 8-mm-wavelength cloud radar (MMCR) to retrieve rainfall profiles above the ACRF sites (e.g., Matrosov et al. 2006). The availability of the W-band ARM cloud radars (WACR) at some ACRF sites offers a possibility of enhancing the attenuation-based approaches.

Remote sensing of rainfall using only the ARM instrumentation provides valuable information, but simultaneous estimates of cloud and precipitation parameters in the same vertical atmospheric column above the ACRF sites are of particular interest. Such retrievals can provide more comprehensive information on the components of the water cycle and shed light on some precipitation formation processes. Independent cloud and precipitation retrieval data could be especially valuable for the purpose of validating the models that separately predict rainfall and cloud contents and their transitions.

This study presents a first attempt for simultaneous retrievals of rainfall parameters and total vertical ice and liquid water cloud amounts in the same vertical column using data available to ARM. These retrievals are mainly based on measurements from the standard instrumentation deployed at the central location of the Southern Great Plains (SGP) ACRF site. The remote sensing approach suggested here is primarily aimed at relatively simple precipitating events such as stratiform ones that exhibit readily identifiable melting-layer features in ARM radar measurements. Stratiform precipitation events typically result in lower-to-moderate rainfall rates $R$ and show only modest variability in $R$ and in the vertical profiles of nonattenuated reflectivity. During such events, MMCR signals usually are not completely attenuated except in the vicinity of cloud tops where reflectivity values are generally very low.

Measurements from ARM microwave radiometers, which are used for estimating integrated liquid amounts in clouds, are not applicable for rainfall conditions because of a variety of factors, including reflector "wetting," multiple scattering effects on raindrops, influences of the melting layer, and the violation of the Rayleigh scattering conditions. Because of that, ARM cloud radars are used for suggested simultaneous retrievals of cloud and rainfall parameters. Measurements from the Weather Surveillance Radar-1988 Doppler (WSR-88D) that is closest to the SGP site are used to estimate total attenuation effects suffered by millimeter-wavelength radars, due to the wet radome and losses in the liquid and melting layers. The ground-based Joss–Waldvogel disdrometer (JWD; Joss and Waldvogel 1967) provides information on rainfall rate and is also used to fine-tune relations between radar and rainfall parameters.

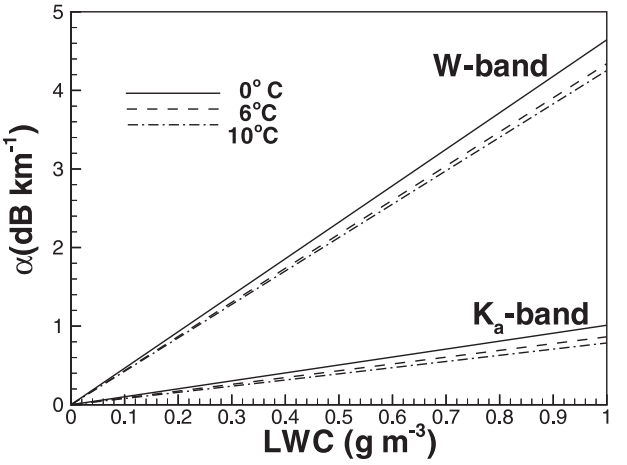


FIG. 1. The $K_a$-band and W-band attenuation coefficients in liquid water clouds as a function of LWC.

## 2. Attenuation of millimeter-wavelength radiation in liquid water clouds and rain

Strong attenuation of millimeter-wavelength radiation in rain and significant non-Rayleigh scattering effects (especially at W band) prevent the use of traditional absolute reflectivity factor (hereinafter just "reflectivity")-based radar methods with MMCR and WACR for retrieving rainfall parameters. For any meteorological radar frequency, these methods cannot be used to discriminate between rain and cloud water if cloud and rain phases coexist in the same radar resolution volume, because the total reflectivity is overwhelmingly dominated by rain. The attenuation-based remote sensing approaches, however, offer a possibility of discriminating between liquid clouds and rainfall.

Unlike radar reflectivities in clouds and rain, which usually differ by several orders of magnitude, attenuations of millimeter-wavelength radiation in liquid clouds and rain are not that dissimilar, especially if rain is not very heavy. For cloud drop sizes, which are typically less than 100 $\mu$m, the Rayleigh approximation is valid, and the cloud attenuation coefficient $\alpha_c$ is linearly dependent on liquid water content (LWC; e.g., Stepanenko et al. 1987):

$$\alpha_c\,(\mathrm{km}^{-1}) = 0.6\pi\lambda^{-1}\,\mathrm{Im}[-(m^2-1)(m^2+2)^{-1}] \times \mathrm{LWC}(\mathrm{gm}^{-3}), \quad (1)$$

where $\lambda$ is the wavelength (cm) and $m$ is the complex refractive index of water, which depends on temperature. For representative temperatures, Fig. 1 shows $\alpha_c$ as a function of LWC for the MMCR (i.e., 34.6 GHz) and WACR (i.e., 94 GHz) frequencies. The temperature dependence of $m$ was adopted from Stepanenko et al.

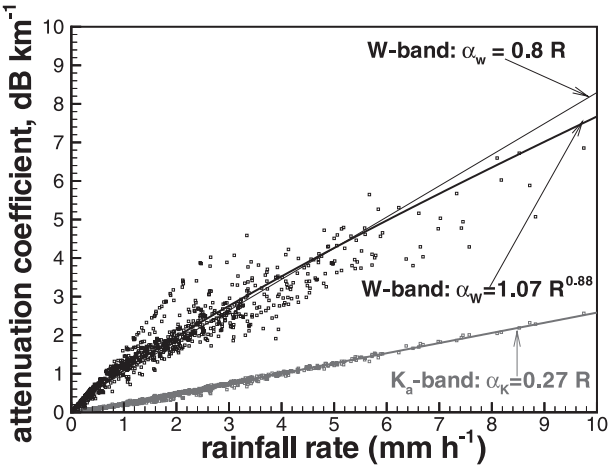


FIG. 2. Scatterplots of W-band and $K_a$-band attenuation coefficients in rain vs rainfall rate for DSDs observed at the SGP site on 1 May 2007.

(1987). Note that typical LWC values observed in midlatitude nimbostratus stratiform precipitating clouds are about 0.2–0.3 g $m^{-3}$ (Mazin 1989).

It can be seen from Fig. 1 that the cloud attenuation at W band is about 5 times that at $K_a$ band, and there is some dependence on temperature. The W-band:$K_a$-band attenuation ratio in rain is only about a factor of 3 on average (as seen in Fig. 2 for rain rates greater than about 0.5 mm $h^{-1}$), mostly due to non-Rayleigh scattering effects, which are already present at W band for drops that are greater than a few hundred micrometers. The spectral difference between the cloud/rain attenuation ratios results in the fact that for a given $R$-to-LWC ratio a fraction of cloud attenuation in the total rain + cloud attenuation is larger at W band by about 65% in comparison with $K_a$ band.

Figure 2 shows the attenuation coefficient in rain $\alpha_r$ as a function of rainfall rate $R$ for normal atmospheric conditions. The rainfall rate and attenuation data in Fig. 2 represent the calculations using the surface JWD data on drop size distributions (DSD) that were collected in 20 size bins every minute during a stratiform precipitation event observed at the SGP site on 1 May 2007. These DSDs were corrected for ''dead time'' effects using the procedure outlined by Sheppard and Joe (1994). The **T**-matrix approach (e.g., Barber and Yeh 1975) was used for calculations of $\alpha_r$. A nonspherical model for raindrops with aspect ratios according to Brandes et al. (2005) and the vertical viewing geometry were assumed for these calculations.

At $K_a$ band, the attenuation coefficient in rain and the rainfall rate are proportional approximately to the same moment of DSD (e.g., Matrosov et al. 2006), and therefore the $\alpha_r$–$R$ relation is practically linear and there is no significant data scatter due to the DSD variability. At W band, the corresponding relation is slightly nonlinear and there is some data scatter due to DSD variations. The best-fit approximation can be given as

$$\alpha_r\ (\text{dB km}^{-1}) = 0.27R\ (\text{mm h}^{-1}; \text{K}_a\text{band}) \quad \text{and} \quad (2a)$$

$$\alpha_r\ (\text{dB km}^{-1}) = 1.07R^{0.88}\ (\text{mm h}^{-1}; \text{W band}). \quad (2b)$$

For $R > 0.5$ mm $h^{-1}$, the relative standard deviations (RSD) of individual data points around the best-fit curves are 5% and 16% for $K_a$ and W bands, respectively. Note that for this case the data scatter for W band is noticeably larger for $R > 6$ mm $h^{-1}$ relative to lower rain rates.

The nonlinearity of the $\alpha_r$–$R$ relation at W band is modest for a common interval of rainfall rates typically observed in stratiform precipitation ($R < 15$ mm $h^{-1}$), and therefore a linear relation could suffice for many practical cases (especially if a particular DSD is not known):

$$\alpha_r\ (\text{dB km}^{-1}) = 0.8R\ (\text{mm h}^{-1}; \text{W band}). \quad (3)$$

For the data shown in Fig. 2, the use of the linear relation (3) instead of (2b) results only in a slight RSD increase (around 18% vs 16%). Note also that the mean relation (3) found here using DSDs for this particular event is practically identical to the one found in Matrosov (2007), where a much wider DSD dataset was used.

Unlike for $\alpha_c$–$R$ relations, there is no significant temperature dependence in the parameters of $\alpha_r$–$R$ relations. It is explained by the fact that several higher-order terms in the **T**-matrix series expansions for the extinction cross sections increase with temperature, which balances the decrease of the first term with temperature (Matrosov 2005). Note that only the first term is responsible for the Rayleigh regime attenuation, and so there is a decrease in the cloud attenuation coefficient $\alpha_c$ when temperature increases.

## 3. Description of the remote sensing approaches

### *a. Estimations of parameters in the liquid hydrometeor layer*

As was shown in the previous section, attenuation of WACR signals in liquid water clouds is about 5 times the attenuation of MMCR signals. On the other hand, the ratio of W- and $K_a$-band attenuations in rain is only about a factor of 3. The difference in the rain and cloud attenuation ratios allows independent estimations of rainfall rate and liquid water amount using the attenuation-based approach applied to dual-wavelength radar measurements.

After integrating equations for attenuation coefficients in a vertical layer of stratiform rain, which also contains liquid water clouds, the following system of equations can be written in terms of mean layer rainfall rate $R_m$ and the liquid water path (LWP):

$$\Delta Z_W = 2C_W R_m \Delta h + 2B_W \times \mathrm{LWP} + G_W \quad \text{and} \quad (4a)$$

$$\Delta Z_K = 2C_K R_m \Delta h + 2B_K \times \mathrm{LWP} + G_K. \quad (4b)$$

In (4), $\Delta Z_K$ and $\Delta Z_W$ are the observed reflectivity differences at $K_a$ and W bands (dB) between the beginning and the end of the considered path interval $\Delta h$ (km), and $G_K$ and $G_W$ are the two-way gaseous absorptions terms. It can be seen from (1) that, if $\Delta Z_K$ and $\Delta Z_W$ are in decibel units and LWP is in grams per meter squared, the coefficients $B_K$ and $B_W$ in (4) can be expressed as

$$B_i = 0.0026\pi\lambda_i^{-1}\ \mathrm{Im}[-(m^2-1)(m^2+2)^{-1}], \quad (5)$$

where the subscript $i$ refers to either W or K frequency band.

To account for changes in raindrop fall velocities with changing air density $\rho_a$, the correction factor $b = (\rho_{am}/\rho_{a0})^{0.45}$ is introduced for rainfall coefficients $C_K$ and $C_W$ as follows:

$$C_K = 0.27b \quad \text{and} \quad C_W = 0.8b, \quad (6)$$

where $\rho_{am}$ and $\rho_{a0}$ are the mean air density for the considered rain layer and the air density for the normal atmospheric conditions, respectively. The gaseous attenuation of millimeter-wavelength radar signals is dominated by water vapor and, to a lesser extent, oxygen. The terms $G_K$ and $G_W$ in (4) are calculated by assuming a linear temperature gradient in the rain layer between the freezing level and the ground and a 90% relative humidity in this layer.

The MMCR operates in several modes that are optimized for different kinds of targets (Kollias et al. 2007). Estimates of $\Delta Z_K$ in the rain layer need to come from the precipitation mode, because measurements of rainfall in other modes are often saturated (at least near the ground) and also the upper bound of the Nyquist velocity interval in other modes is smaller than typical Doppler velocities observed in rainfall. This can cause larger uncertainties in reflectivity difference estimates using these other modes because reflectivity is estimated by integrating over the Doppler spectrum. The Nyquist interval for the MMCR precipitation mode is $\pm 20.28$ m s$^{-1}$, which is suitable for rain measurements. Because of stronger non-Rayleigh scattering at W band (e.g., Lhermitte 2002), the vertical Doppler velocities measured by WACR are noticeably smaller than those from MMCR (about 4–4.5 vs about 7–7.5 m s$^{-1}$), and therefore the general WACR measurement mode with the Nyquist interval of $\pm 7.9$ m s$^{-1}$ should be adequate for estimates of $\Delta Z_W$.

Equations (4) assume that the attenuation in rain and cloud liquid is the dominant factor responsible for vertical changes in the observed reflectivity. This assumption is generally valid for millimeter-wavelength vertical measurements in stratiform rain where the vertical variability of rainfall rate is usually modest and so are vertical changes in nonattenuated reflectivity (e.g., Bellon et al. 2005; Matrosov et al. 2007). At the same time, changes of observed reflectivity values with range caused by attenuation are substantial. These changes become more pronounced as the vertical thickness of the rain layer increases. Note also that the non-Rayleigh scattering effects at $K_a$ band and especially at W band (Matrosov 2007) further diminish possible changes in nonattenuated reflectivity of rain (relative to nonattenuated reflectivities at centimeter radar wavelengths), thus further reducing contributions from varying nonattenuated reflectivity to the retrieval uncertainty of the attenuation-based method.

One approach for simultaneously estimating $R_m$ and LWP in the layer containing rain and liquid water clouds is to solve the system of linear equations in (4) for these parameters. Another approach is to use rainfall-rate information available from JWD measurements and then to retrieve LWP by minimizing observed reflectivity differences under the assumption that the surface rainfall is representative of the mean layer rainfall for the stratiform rain. The working experience with SGP data indicates that the retrieval results from solving the system (4) are sometimes noisy, which might be caused by some artifacts in the MMCR precipitation mode data (P. Kollias and S. Giangrande 2008, personal communication). At W band, the total attenuation by rain and liquid clouds is higher and the variability of nonattenuated reflectivities is lower. Given this, the current study is focused on the second approach mentioned above, under which the LWP estimates are obtained from

$$\mathrm{LWP} = (\Delta Z_W - 2C_W R_m \Delta h - G_W)(2B_W)^{-1}, \quad (7)$$

where $R_m$ estimates come from the JWD data.

### b. Identifying rain layers

An important issue is identifying the vertical boundary of the liquid hydrometer layer, which contains rain and liquid water clouds. In stratiform precipitating systems, the rain layer is typically separated from the ice phase by the melting layer, which is about 400–500 m

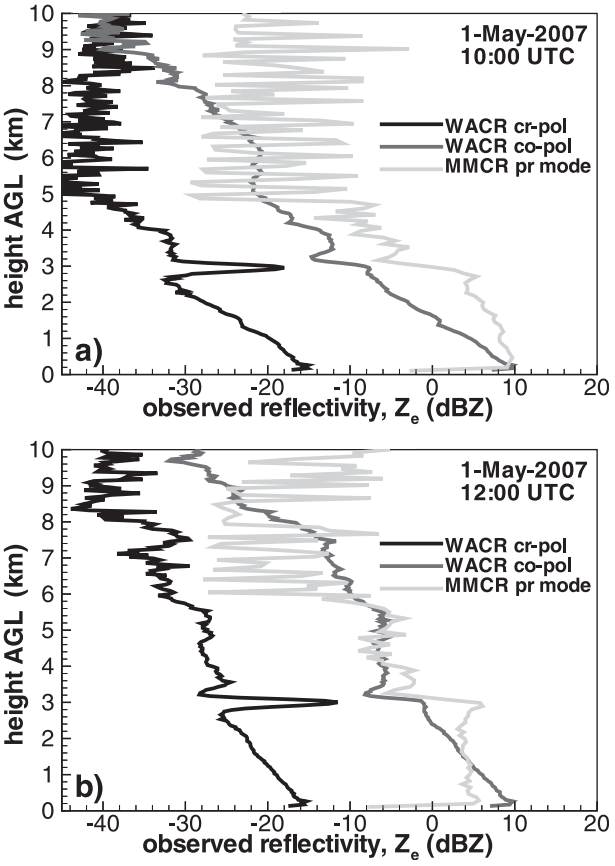


FIG. 3. Vertical profiles of MMCR (precipitation mode) and WACR reflectivities observed during the stratiform rain event on 1 May 2007: (a) 1000 and (b) 1200 UTC.

thick. In MMCR measurements, the melting layer can be identified by a few-decibel reflectivity enhancement, which is caused by melting ice particles. Figure 3 shows examples of vertical profiles of MMCR and WACR reflectivity measurements taken during an SGP precipitating event observed on 1 May 2007. MMCR data exhibit a weak reflectivity maximum in the melting layer.

Polarimetric WACR data provide a robust way of identifying the boundary between the melting and rain layers. This radar operates on a linear polarization basis and measures copolar and cross-polar echoes. Kollias and Albrecht (2005) show that for ground-based W-band radars the copolar reflectivities cannot be used to identify the melting layer. However, the cross-polar measurements, as seen in Fig. 3, can serve as an indicator of this layer. A very pronounced cross-polar signal enhancement is explained by highly depolarizing scattering by melting ice particles. The WACR cross-polar data show that for both examples in Fig. 3 the upper/lower boundary of the rain/melting layer is located at about 2.6 km above ground level (AGL). The freezing level, which is also identifiable from these data, is located at about 3.1 km AGL.

It is further assumed that the liquid water clouds (if any) are present only in the rain layer. Although supercooled liquid water can potentially be present above the freezing level, its contribution to the total LWP is currently neglected. Note also that the MMCR vertical Doppler velocity measurements in the ice/snow regions can serve as an indicator of significant ice crystal riming (Matrosov et al. 2008b). The values of these velocities, which are less than about 1.6 m $s^{-1}$, suggest no or little riming and, hence, a lack of significant amounts of supercooled water.

The lower boundary of the liquid layer is determined by the lowest height at which cloud radar echoes are not saturated [i.e., liquid clouds (if any) that exist lower than this boundary are not included in retrievals]. For low and moderate rainfalls, this lower boundary usually corresponds to the third (or second) range gate for both WACR copolar mode and MMCR precipitation mode. Note that special attenuators are used for the MMCR precipitation mode to mitigate the saturation effects in rain observed at closer ranges. Because of these attenuators, the MMCR precipitation mode cannot reliably detect cloud returns at altitudes higher than 5 km (at 1000 UTC; Fig. 3) and 6 km (at 1200 UTC). There is a similar lack of sensitivity in the WACR cross-polar mode for which rain echoes are 25–26 dB lower than in the copolar mode.

### c. *Estimations of the ice cloud properties above the freezing level*

Ice parts of precipitating cloud systems are of a particular interest because ice particle melting is one of the mechanisms of raindrop formation. A quantitative interpretation of ground-based cloud radar echoes from these cloud parts, however, is not very straightforward because of the attenuation of signals in the rain and melting layers and by wet radome. Unlike for liquid phase, attenuation-based approaches are not practical for ice phase because of small attenuation of radar signals in dry ice. No available ground-based optical instruments can efficiently be used for such clouds; thus, cloud radar measurements are still the best hope for ice-phase retrievals.

Because ice-phase retrievals should rely on absolute radar measurements, corrections for the signal attenuations need to be introduced. Such corrections can potentially be made based on the rain-layer retrievals of $R_m$ and LWP and on a theoretical consideration of the signal propagation in the melting layer (e.g., Matrosov 2008), but some additional factors such as the wet radome attenuation are very difficult (if not impossible) to

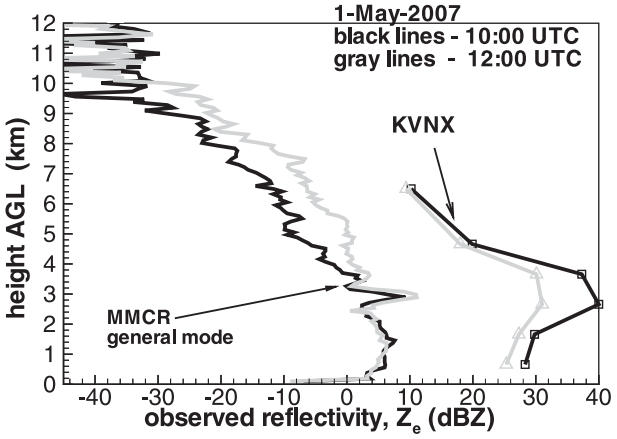


FIG. 4. Comparisons of MMCR (precipitation mode) and KVNX reflectivity observed during the stratiform rain event on 1 May 2007: 1000 (black lines) and 1200 (gray lines) UTC.

account for in an accurate quantitative manner. Given this, it appears practical to introduce corrections to the absolute reflectivities observed by the ARM radars based on using data available from nearby longer-wavelength radars.

It was suggested earlier (albeit for nonprecipitating cloud studies) that National Weather Service radars can supplement ARM radar observations (e.g., Miller et al. 1998). One such WSR-88D, which is part of the Next Generation Weather Radar (NEXRAD) network, is located at the Kegelman Airfield in northern Oklahoma. This radar has the four-letter site identifier KVNX and is the closest NEXRAD to the ARM SGP site. The WSR-88D operates at S band ($\lambda \sim 10$ cm), and attenuation of their signals is negligible in most practical cases. During precipitation events the KVNX radar performs volume scans that can be used to estimate low-spatial-resolution vertical profiles of nonattenuated reflectivity over the SGP site approximately every 6 min.

As an illustration, two reconstructed profiles of the KVNX reflectivity over the SGP central facility are shown in Fig. 4. For comparison, profiles of the general-mode MMCR reflectivity are shown for the same times. The MMCR measurements in this mode are significantly more sensitive than those in the precipitation mode, and signal saturation is evident up to the heights of about 1.5 km AGL. The general mode has a Nyquist interval of $\pm 5.1$ m s$^{-1}$ and is appropriate for observing the ice parts of precipitating cloud systems. The large difference between KVNX and MMCR data is caused primarily by the hydrometeor and wet radome attenuation.

The KVNX radar is located at a distance of about 60 km from the SGP central facility in an azimuthal direction of 285°. The cross-beam resolution of the KVNX radar at this distance is about 1 km and the data along the beam are sampled at 1-km range (at the legacy resolution), which results in about a 1-km$^3$ volume resolution above the MMCR. For a particular range, the KVNX scanning routines, which might differ from event to event, provide reflectivity data centered only at a few heights that are lower than 10 km AGL. Note that the beam for the lowest KVNX measurements in the direction of the SGP may be partially blocked. The coarse resolution of the KVNX radar results in a vertically expanded melting-layer reflectivity enhancement relative to the MMCR measurements. For this event, the two KVNX measurements centered at $h_1 \approx 4.8$ km and $h_2 \approx 6.6$ km AGL should be free of melting-layer influences, although for shallower precipitation the KVNX resolution volume centered at 6.6 km can be filled only partially by hydrometeors.

Because there are only a few KVNX measurements (sometimes only one ''good'' data point) over the SGP site above the freezing level, this radar is not well suited for vertical ice water amount retrievals. However, the S-band KVNX reflectivity measurement $Z_{es}(h_1)$ centered at height $h_1$ can be used to estimate the combined effects of rain, melting layer, gases, and wet radome attenuations suffered by the MMCR radar echoes. The MMCR attenuation correction procedure for MMCR reflectivities observed in the ice parts of precipitation clouds included vertical averaging of MMCR general-mode reflectivities to match the vertical resolution of the KVNX radar. The resulting mean observed MMCR value $Z_{em}(h_1)$ was compared with the corresponding KVNX radar value, and an offset $\Delta Z$ was determined as

$$\Delta Z = [Z_{es}(h_1) - \Delta Z_{s-k}] - Z_{em}(h_1), \tag{8}$$

where $\Delta Z_{s-k}$ is a correction for the S band minus $K_a$ band reflectivity difference due to non-Rayleigh scattering.

Figure 5 shows the correspondence of S- and $K_a$-band reflectivities as calculated using a large ice cloud microphysical dataset (Heymsfield et al. 2005) as discussed by Matrosov and Heymsfield (2008). It can be seen that the S band minus $K_a$ band difference is small for $Z_{es} < 0$ dB$Z$, but it is around 6 dB for $Z_{es} \sim 20$ dB$Z$. Overall, the following polynomial approximation (which is also shown in Fig. 5) can be used for the term $[Z_{es}(h_1) - \Delta Z_{s-k}]$ in decibel units:

$$(Z_{es} - \Delta Z_{s-k}) = -0.62 + 0.904 Z_{es} - 0.007\,20 Z_{es}^2 - 0.000\,187 Z_{es}^3. \tag{9}$$

It can be seen from Fig. 5 that there is some data scatter around the best polynomial fit of the relation between S-band and $K_a$-band reflectivities. The standard deviation

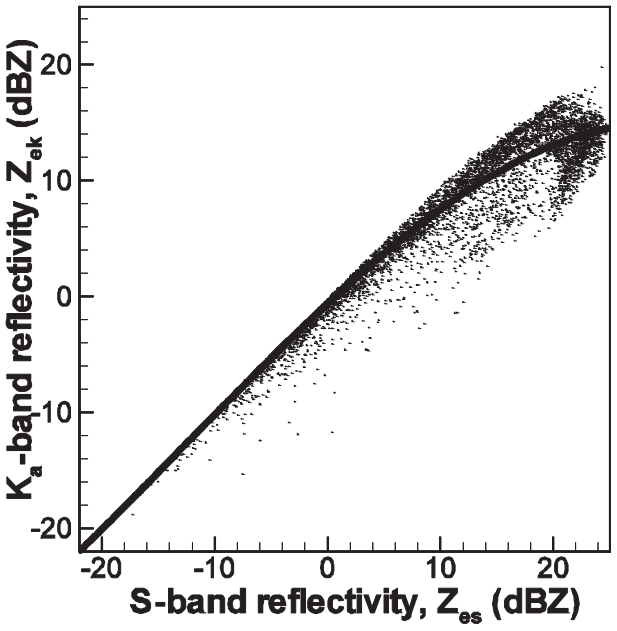


FIG. 5. A scatterplot of S-band vs $K_a$-band nonattenuated reflectivities calculated using a wide range of ice particle experimental size distributions. The best-fit polynomial approximation is also shown.

of the data scatter is about 1.5, 1.9, and 2.3 dB for the $Z_{es}$ levels of 10, 15, and 20 dB$Z$, correspondingly.

The corrected offset $\Delta Z$ is then applied to the MMCR reflectivities observed above the freezing level at the time of the KVNX reflectivity measurement. Six-minute time averaging of MMCR data was also performed to match the time resolution of the KVNX measurements and to mitigate, in part, effects of differing horizontal resolutions of the radars.

The corrected MMCR reflectivity profiles are then used to estimate ice water content (IWC) and its vertical integral—ice water path (IWP). A relation for ice regions of precipitating systems (Matrosov and Heymsfield 2008),

$$\mathrm{IWC}\ (\mathrm{g\ m^{-3}}) \approx 0.06 Z_e^{0.8}\ (\mathrm{mm^6\ m^{-3}}), \qquad (10)$$

is used for these estimations. This relation is in general agreement with data presented by Protat et al. (2007, their Fig. 1). No significant temperature dependence in coefficients of the IWC–$Z_e$ relation was found for the high values of $Z_e$ that are typical in these regions.

## 4. Evaluation of the KVNX data

The procedure described above for the correction of MMCR general-mode reflectivities relies on the assumption that the KVNX data are well calibrated. It is instructive to check the KVNX calibration both in the

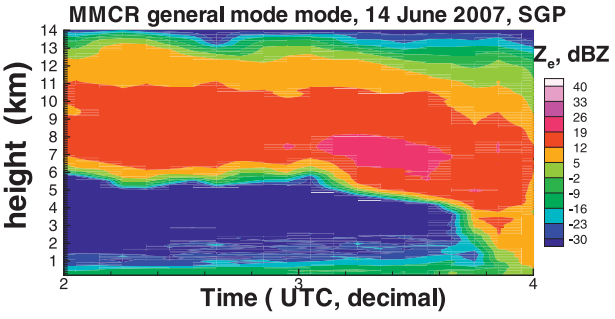


FIG. 6. A time–height cross section of the thick nonprecipitating ice cloud observed by the MMCR at the SGP central facility on 14 Jun 2007.

absolute sense and in a relative sense as compared with the MMCR calibration. The latter check can be performed by simultaneously observing with both radars thick ice clouds, which are similar in reflectivity to ice parts of precipitating clouds, but are observed without intervening liquid and melting layers that cause attenuation of MMCR signals. One such cloud, which was relatively homogeneous in the horizontal direction and located entirely above the freezing level, was observed by the MMCR over the SGP site between 0200 and 0330 UTC 14 June 2007 as shown in Fig. 6. The volume scans of the KVNX radar on this date included measurements that were centered at about 8.5 km AGL above the SGP site. At this altitude, KVNX measurements were centered in the middle of the cloud where vertical gradients of MMCR reflectivity were the smallest.

Figure 7 shows time series of comparisons of KVNX and general-mode MMCR data that were averaged to match the KVNX resolution over the SGP site. Both types of measurements generally follow each other, and the mean difference between KVNX and MMCR reflectivities is about 3.8 dB. It can be calculated from (8) that an average difference between S- and $K_a$-band reflectivities is expected to be around 5.5 dB for this level of observed reflectivities. Given a standard deviation value of about 2.3 dB in data scatter in Fig. 5, it can be concluded that MMCR and KVNX reflectivity data are mutually consistent, although a positive offset of around 1.7 dB of MMCR data relative to the KVNX data cannot be ruled out.

The absolute calibration of the KVNX radar data can also be checked by comparing measured NEXRAD reflectivities in the rain layer with independent estimates of these reflectivities. Such independent estimates can be obtained from calculations using the JWD DSDs collected during a rain event. Figure 8 shows comparisons of KVNX and JWD reflectivity values for the event observed on 1 May 2007. The presented KVNX data were centered at about 1.66 km AGL (i.e., the only

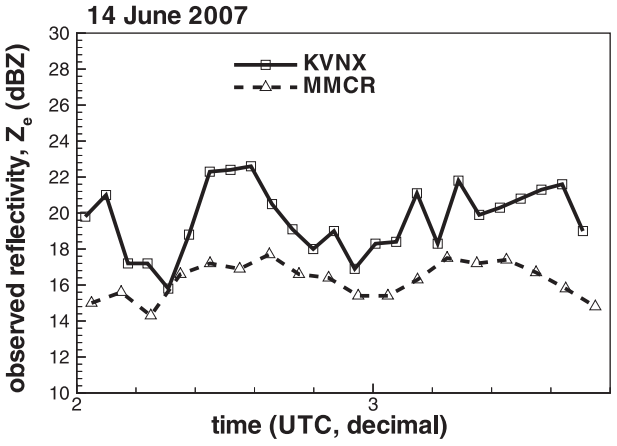


FIG. 7. Nonprecipitating ice cloud comparisons of KVNX reflectivities over the SGP central facility centered at 8.5 km AGL with MMCR general-mode measurements averaged to match the KVNX resolution.

measurement that was fully within the rain layer for this event and unaffected by potential beam blockages) over the SGP site. The JWD data were ''dead-time corrected'' and averaged in 6-min intervals to alleviate sampling volume differences and to approximately match KVNX measurement times. It can be seen that there is generally good agreement between both datasets. Although there are periods during which KVNX (or JWD) data exceed JWD (or KVNX) values by a few decibels that can be in part due to some vertical rainfall variability and also due to differences in resolution volumes of the instruments, an average negative bias of KVNX reflectivities is only about 1.3 dB.

The robustness of JWD rainfall DSD estimates (and hence rain reflectivity estimates) is also indirectly confirmed by very good agreement between the rainfall accumulations calculated from JWD rainfall rates and data from the standard tipping-bucket rain gauge, which is deployed near the JWD. The corresponding comparisons of rainfall accumulations are shown in Fig. 8b. These results also indicate the improvement of the JWD accumulation estimates when the dead-time correction for measured raindrop spectra is introduced. Overall it can be concluded that KVNX measurements are in decent agreement with nonattenuated MMCR by liquid-phase general-mode data (at least for this observational case). Although potential biases of 1–2 dB cannot be ruled out, such reflectivity uncertainties are common for the meteorological radars.

## 5. A case study

A stratiform precipitating event observed on 1 May 2007 at the SGP site provides a good illustration for an

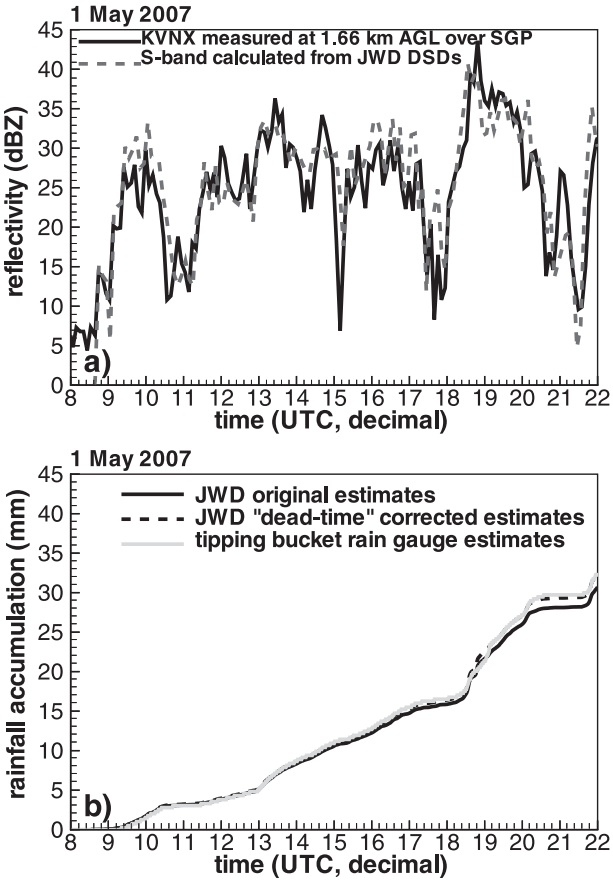


FIG. 8. Comparisons of the (a) S-band reflectivities measured in the rain layer by the KVNX WSR-88D and calculated from JWD DSDs and (b) rainfall accumulations from the tipping-bucket gauge and JWD.

application of the suggested remote sensing method. The time–height cross sections of radar reflectivities observed by the ARM vertically pointing radars and the KVNX S-band radar are shown in Fig. 9. As previously mentioned, the ARM radar data were averaged in 6-min intervals. The melting layer was observed approximately between 2.7 and 3.2 km, and its height was relatively stable during the event. The WACR copular-mode data were not totally attenuated up to the highest levels of the liquid hydrometeor layer. The upper boundary of this layer is identifiable by the reflectivity maxima in the MMCR general-mode data (Fig. 9a), cross-polar maxima of the WACR data (Fig. 9c), and the Doppler velocity transition (Fig. 9e).

The observed (not attenuation corrected) WACR copolar data between 2.7 and 0.2 km (i.e., $\Delta h = 2.5$ km) were used for retrievals of LWP according to (7). The time series of these values are shown in Fig. 10. The MMCR general-mode reflectivities (Fig. 9a) were then corrected for attenuation by means of KVNX

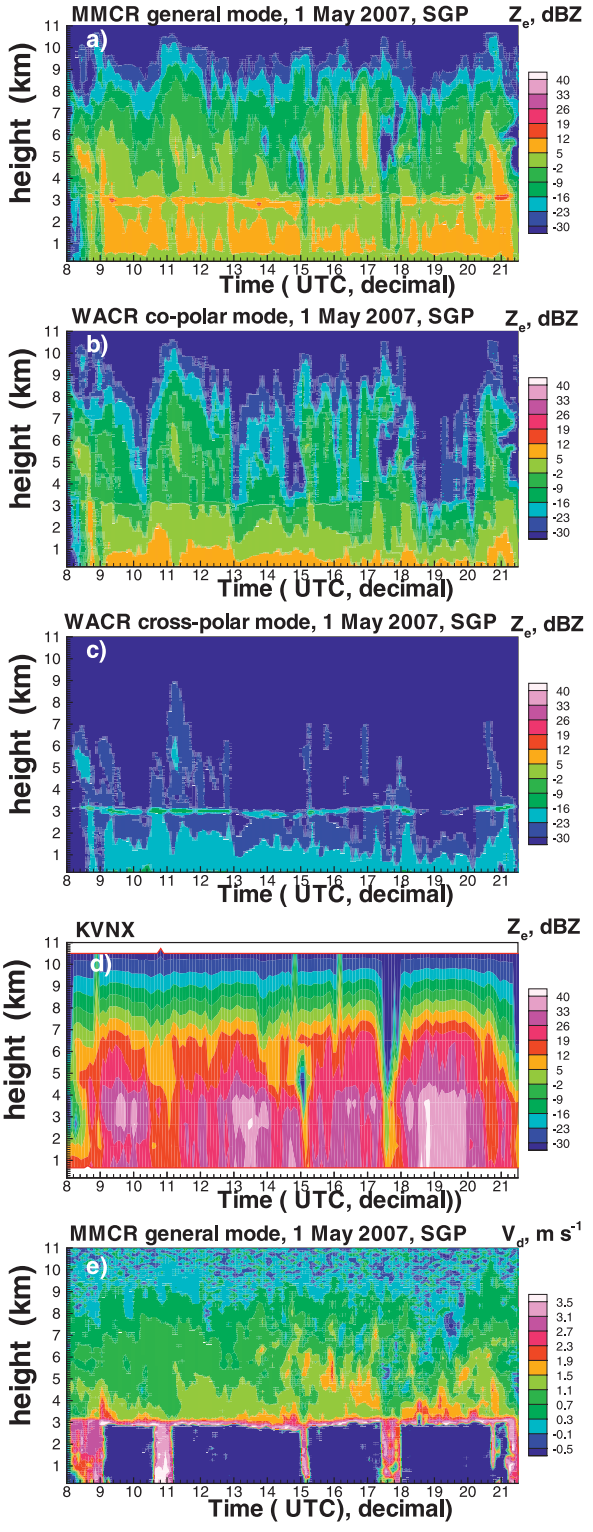


FIG. 9. Time–height cross sections of radar reflectivities observed at the SGP site on 1 May 2007 by the (a) MMCR general mode, WACR (b) copolar and (c) cross-polar modes, and (d) KVNX WSR-88D. (e) The MMCR general-mode Doppler velocities, which are aliasing in the rain region.

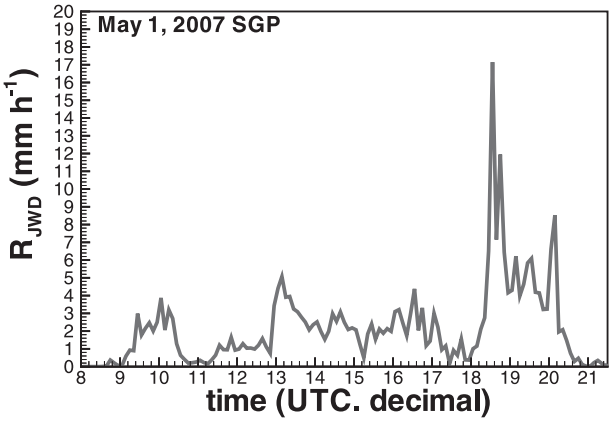


FIG. 10. Time series of rainfall rate calculated from JWD data for the 1 May 2007 SGP event (6-min averages).

measurements above the freezing level at 4.7 km AGL and were used to retrieve IWP. There were two more KVNX measurements in the ice part during this event, which corresponded to the heights of 6.6 and 10.5 km AGL. The 10.5-km measurements were often near the noise floor, and 6.6-km data could have some beam-filling issues, and so the approximated reflectivities in the upper part of the echo ($h > 6$ km) in Fig. 9d might not be very reliable.

More significant attenuation in the liquid layer is evident in the 3.2-mm WACR data when compared with the longer-wavelength ($\lambda \sim 8.7$ mm) MMCR data (Fig. 9a vs 9b). The MMCR-measured echo extends higher. Some MMCR general-mode returns near the cloud tops can be completely attenuated out. This fact, however, is not likely to significantly bias ice content estimates for lower-to-moderate rain rates because typically more than 85%–90% of the total cloud IWP in precipitating systems comes from the lower part of an ice-phase region where nonattenuated reflectivity values exceed 0 dB$Z$ (e.g., Matrosov and Heymsfield 2008). The maximum KVNX-based attenuation correction for the MMCR general-mode measurements in the ice region was about 33 dB at around 1830 UTC when the heaviest rainfall was observed (see Fig. 11). This correction was about 20 dB for more typical rainfall at about 1600 UTC. Because the MMCR sensitivity in this mode is about −33 dB$Z$ at a 10-km height, it means that only ice cloud parts with nonattenuated reflectivities that were less than 0 dB$Z$ were missed during the heaviest rainfall (and less than about −13 dB$Z$ during typical rainfall).

Except for a few pockets, vertical Doppler velocities $V_D$ observed above the freezing level (Fig. 9e) are generally less than 1.5–1.6 m s$^{-1}$, which indicates no significant crystal riming (Mosimann 1995) and hence no significant amount of supercooled liquid water. Note

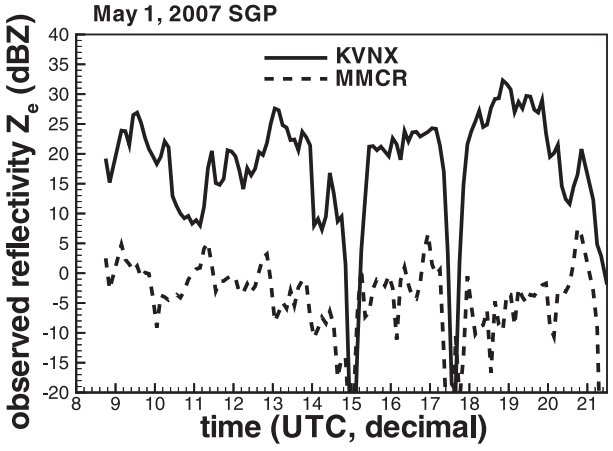


FIG. 11. Time series of observed KVNX (solid line) and MMCR (dashed line) reflectivities centered at 4.8 km AGL. MMCR reflectivities were vertically averaged to match the KVNX resolution (6-min averages).

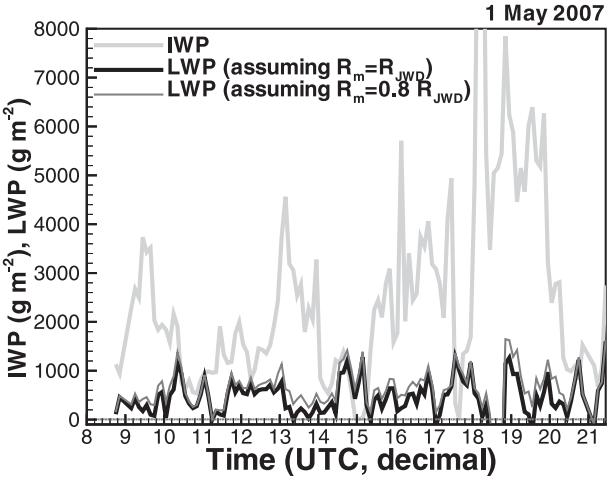


FIG. 12. Retrievals of IWP and LWP for the 1 May 2007 stratiform precipitation event.

that $V_D$ values in rain are aliased (folded) because the Nyquist velocity in the MMCR general mode is generally less that typical fall velocities of raindrops. Doppler velocity data (as do JWD data in Fig. 10) indicate that appreciable rainfall lasted generally from 0900 to 2100 UTC except for several short interruptions at around 1100, 1500, and 1730 UTC when $V_D$ values in the liquid hydrometer layer were generally less than 3.5 m s$^{-1}$, which might correspond to light drizzle.

Figure 11 shows time series of the KVNX reflectivities above the MMCR centered at 4.7 km AGL and the corresponding MMCR attenuated reflectivities averaged to match the KVNX resolution. The two brief periods of no rain at around 1530 and 1730 UTC also corresponded to pronounced decreases in the ice cloud reflectivities as observed by both radars. A substantial ice cloud was, however, present during the period of no significant rain at around 1100 UTC. At the end of this period, the KVNX − MMCR difference was about 3–4 dB, as expected from the non-Rayleigh scattering effects at an ~10-dB$Z$ reflectivity level (see Fig. 5) observed by the KVNX radar. Wet radome effects, which gradually diminished toward the end of this no-rain period, were a likely cause of higher KVNX–MMCR differences in the beginning of this period.

Times series of IWP and LWP retrievals are shown in Fig. 12. The presented retrievals, as with the JWD data in Fig. 10, are 6-min averages. It can be seen that IWP values as a rule are significantly larger than LWP values in the same vertical column. Over the course of the event, both LWP and IWP varied significantly. The rainfall was mostly light to moderate with an average value for the rain rate of about 3.8 mm h$^{-1}$. To assess a sensitivity of LWP results to $R_m$ uncertainties, retrievals using (7) were performed assuming $R_m = R_{\rm JWD}$, and also assuming that $R_m$ differs from $R_{\rm JWD}$ by 20%. The time series for both assumptions are depicted in Fig. 12.

There are no direct comparisons available for the retrieved values of LWP and IWP with independent estimates of these quantities. Microwave radiometer–based approaches to estimate LWP, which are used by ARM for nonprecipitating clouds, are not applicable for precipitating cases. The Vaisala ceilometer deployed at the SGP site provides measurements of the cloud lower boundary. Although the reliability of these measurements in rainy conditions is not exactly known, the ceilometer information can perhaps still be used qualitatively as an indicator of the probable presence of the liquid clouds in the vertical column below the freezing level.

Figure 13 shows time series of cloud-base heights as detected by the ceilometer. The LWP retrievals are also shown. It can be seen that clouds in the rain layer (i.e., between 0 and 2700 m) were detected for almost the whole period of the observational event, except for short periods at around 0830, 0930, and 1330 UTC. These are also the times when the radar attenuation–based retrievals exhibit minima in LWP retrievals. The ARM micropulse lidar data on cloud boundaries for this event (not shown) were similar to the ceilometer data.

## 6. Estimation of retrieval uncertainties

### *a. Estimations of uncertainties of $R_m$ and LWP*

The method uses estimates of the surface rainfall rates from the JWD measurements as a proxy for the mean rainfall rate in a layer between the ground and the melting layer. These surface estimates are robust and provide a very good accumulation agreement with the

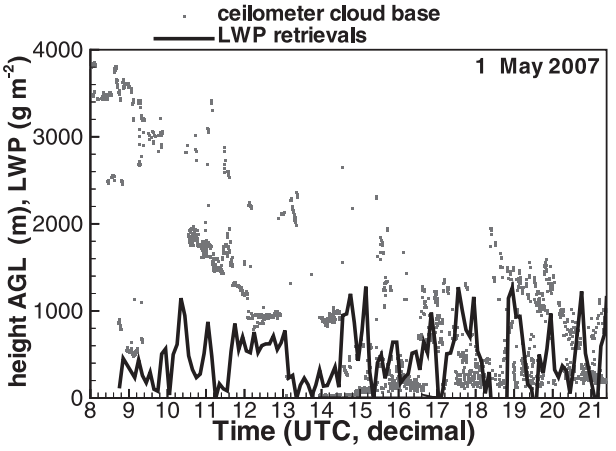


FIG. 13. Times series of LWP retrievals and ceilometer estimates of the cloud-base heights.

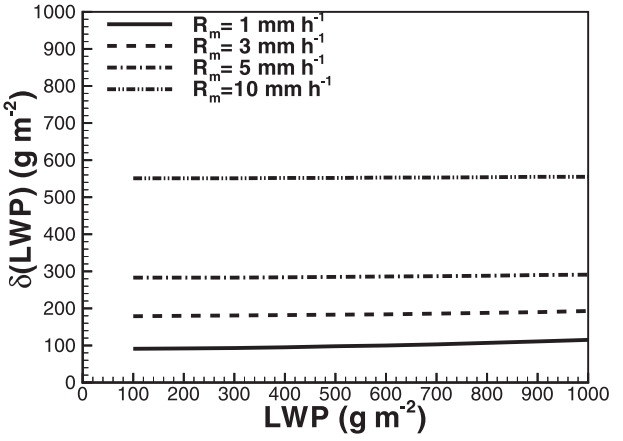


FIG. 14. Estimates of the LWP retrieval uncertainties.

standard rain gauge measurements (see Fig. 8b). A certain vertical variability of rainfall is usually present even for stratiform events, but it is expected to be relatively modest. Although evaporation processes tend to decrease rainfall rate with decreasing height AGL, cloud drop washout by raindrops can counteract these processes. Observations with centimeter-wavelength radars (e.g., Bellon et al. 2005; Matrosov et al. 2007) indicate that the variability in vertical profiles of nonattenuated reflectivity in stratiform rainfall is modest (typically ~1–1.5 dB). Note that this variability is primarily due to changes in rainfall and not in liquid water clouds because (unlike for attenuation coefficients, which usually are of the same order of magnitude for clouds and rain) nonattenuated reflectivity of rainfall is usually several orders of magnitude greater than that of liquid water clouds. Typical exponent values $d$ in the centimeter-wavelength $Z_e$–$R$ relations ($Z_e = cR^d$) are about 1.3–1.8, and so it can be estimated that an approximately 20% variability in $R$ could cause typical variabilities in $Z_e$ (i.e., ~1–1.5 dB). Thus it is further assumed that the use of surface value of $R_{\mathrm{JWD}}$ as a substitute for the layer mean rainfall rate $R_m$ has a 20% uncertainty.

It can be seen from (7) that errors of LWP estimations will depend on uncertainties of $\Delta Z_W$, $G_W$, and $B_W$ and the uncertainties of the total rainfall attenuation, which is given by the term $A_R = 2C_W R_m \Delta h$. Assuming independence of these contributions, one can estimate them as

$$\delta(\mathrm{LWP})_{\Delta Z} = \delta(\Delta Z_W)(2B_W)^{-1}, \quad (11a)$$

$$\delta(\mathrm{LWP})_G = \delta(G_W)(2B_W)^{-1}, \quad (11b)$$

$$\delta(\mathrm{LWP})_B = \delta(B_W)B_W^{-1} \times \mathrm{LWP}, \quad \text{and} \quad (11c)$$

$$\delta(\mathrm{LWP})_A = \delta(A_R)(2B_W)^{-1}, \quad (11d)$$

where $\delta(\Delta Z_W)$, $\delta(G_W)$, $\delta(B_W)$, and $\delta(A_R)$ are uncertainties in $\Delta Z_W$, $G_W$, $B_W$, and $A_R$. The uncertainty in $A_R$ comes from a 20% uncertainty in $R_m$ (as discussed above) and an approximately 18% uncertainty in variability of the W-band attenuation coefficient due to changes in rain DSDs (see Fig. 2). Assuming independence of these two factors, one can conclude that, for a given value of $R_m$, $A_R$ can vary by approximately 27% (i.e., $0.27^2 \approx 0.20^2 + 0.18^2$).

The uncertainty of $B_W$ is primarily from the variability of the mean cloud temperature. This variability of ±6°C would result in $\delta(B_W)B^{-1}{}_W \approx 0.07$. It was further assumed that $\Delta Z_W = 1$ dB and $G_W = 0.5$ dB. The resulting uncertainty of the LWP retrievals can be estimated as

$$[\delta(\mathrm{LWP})]^2 = [\delta(\mathrm{LWP})_{\Delta Z}]^2 + [\delta(\mathrm{LWP})_G]^2 + [\delta(\mathrm{LWP})_B]^2 + [\delta(\mathrm{LWP})_A]^2 \quad (12)$$

if the independence of all of the contributions from (11) is assumed.

Figure 14 shows estimates of $\delta$(LWP) for different values of mean rainfall rate. This rainfall rate is a very significant factor influencing the absolute uncertainties of LWP retrievals. Their dependence on LWP is not very pronounced, though there is a slight increase in $\delta$(LWP) with LWP, which is due to the cloud temperature uncertainty contribution (11c). It can be seen also that for mean conditions observed during the 1 May 2007 event, LWP uncertainties of around 200–250 g m$^{-2}$ can be expected. It means that some of the liquid cloud retrievals with lower LWP can produce unrealistic negative values. Indeed, a few slightly negative retrieved LWP values can be seen in Fig. 12.

### b. Retrieval errors for IWP

IWP retrievals are based on IWC estimates that are obtained from the attenuation-corrected MMCR

general-mode reflectivities using relation (10). The retrieval errors are caused by the uncertainties in reflectivity values and by the uncertainty of the power-law relation between radar reflectivity and cloud microphysical parameters. The later uncertainty could be on average about 70% or so (e.g., Matrosov et al. 2003; Protat et al. 2007). Judging from the results of section 4, the uncertainty of corrected MMCR general-mode reflectivities can be estimated as about 2.5 dB, even after correcting for S band minus $K_a$ band differences. This reflectivity uncertainty translates to an approximately 50% additional uncertainty of IWC estimates. Assuming the independence of these two uncertainties and considering them as variances (i.e., ~70% and ~50%), a total uncertainty could be estimated at around 86%. It can be expected also that IWP estimates can be on average more accurate than individual IWC retrievals because some errors can be canceled out because of the vertical integration of IWC. Overall, a factor-of-2 uncertainty in IWP retrievals could be a plausible estimate. Note also that results from Comstock et al. (2007) indicate that power-law radar reflectivity–based approaches for ice clouds provide reasonable IWP retrievals that compared favorably to multisensor-based methods when these methods were applicable (i.e., no intervening liquid hydrometeor layers).

## 7. Conclusions

Vertically pointing ARM cloud radars, which are operated at W and $K_a$ frequency bands, can be used to obtain IWP of cloud parts above the melting layer and LWP of liquid water clouds coexisting with rainfall below the melting layer in stratiform precipitating systems where polarimetric and Doppler radar measurements offer a clear separation among liquid, mixed, and ice phases of water. Separating the precipitating (i.e., rain) and suspended (i.e., cloud) liquid can be done using estimates of $K_a$- and W-band total attenuations in the liquid hydrometer layer and the frequency differences in rain and cloud attenuation coefficients. The simultaneous retrievals of LWP and rainfall rate using radar-only data can be noisy, but available robust estimates of rainfall from a disdrometer can be used in a version of the attenuation-based method. In this version, LWP retrievals are performed using only layer attenuation estimates at W band where attenuation effects are stronger, nonattenuated reflectivity in a liquid layer containing rain is less variable in the vertical direction, and the liquid cloud contributions to the total attenuation are larger than at $K_a$ band. The attenuation-based LWP estimates are immune to the uncertainties in the radar absolute calibration and the wet radome attenuation because relative (differential) measurements are used.

Parameters of the ice clouds observed above the melting layer are retrieved using 8-mm cloud radar measurements of absolute reflectivity that are corrected for the effects of combined attenuation by the wet radome and by the liquid and melting layers. The MMCR measurements are attenuated in the liquid and melting hydrometeor layers significantly less than WACR measurements and are more suitable for ice-phase estimates. The attenuation correction procedure uses the measurements from the operational WSR-88D that is located near the SGP central facility. The corrected MMCR data provide estimates of vertical profiles of ice water content that are used to calculate columnar values of IWP.

The suggested hydrometeor parameter estimation approach provides time series of mean rainfall rates $R_m$, LWP, and IWP values for the vertical atmospheric column above the ARM SGP central facility. The time resolution of the hydrometeor parameter retrievals is 6 min, which is chosen, in part, because of the time resolution of available WSR-88D data and also to reduce some spatial and temporal variability in the retrieved time series. The suggested approach was applied to a case study observed at the SGP ACRF site on 1 May 2007. This event exhibited well-defined melting layer boundaries, and there was generally little (if any) supercooled liquid water above the freezing level. The rainfall rates during this event varied in a range between 0 and 15 mm $h^{-1}$, with typical values around $R_m \sim$ 3–4 mm $h^{-1}$. LWP estimates were sometimes reaching 1000–1500 g $m^{-2}$, with typical values of about 300–500 g $m^{-2}$. Retrieved values for IWP were noticeably larger than those for LWP and usually exceeded 1000 g $m^{-2}$. Maximum retrieved IWP values were about 10 000 g $m^{-2}$.

LWP retrieved errors depend on the mean layer rainfall rate and are about 200 g $m^{-2}$ for typical values of $R_m$ observed during the case study. These errors increase with $R_m$ and can be as high as about 500 g $m^{-2}$ for $R_m \approx 10$ mm $h^{-1}$. Uncertainties of IWP estimates using an IWC–$Z_e$ relation could be as high as a factor of 2 or even higher, which, however, is not uncommon for the radar-based estimates of ice cloud parameters. Heavier rainfalls with $R_m > 15$ mm $h^{-1}$, which cause total attenuation of MMCR signals at some point within the ice cloud, can result in some negative biases of IWP estimates. Such biases, however, are not expected to be greater than about 10% for $R_m < 15$ mm $h^{-1}$, which is significantly less than the uncertainty of IWP retrievals.

The proposed approach is applicable to established stratiform precipitating events that typically do not exhibit high vertical variability of rainfall and for which the corresponding rainfall rates are generally less then about 15 mm $h^{-1}$. Note also that the spectral dependence of the liquid cloud/rain attenuation ratio for

$R < 0.5$ mm $h^{-1}$ is not very pronounced, so lighter rainfall estimates can have larger errors if the full system (4) is used for retrievals. Precipitating events with possible high vertical variability of rainfall might not be well suited for retrievals using the suggested method. Such events, however, are usually recognizable by slant patterns of observed reflectivity (Matrosov et al. 2006). It is not clear how applicable the suggested approach will be for convective precipitation when an obvious vertical separation of ice, mixed (i.e., melting), and liquid phases is not readily available and the vertical variability of rainfall could be significant. Future plans include multiple retrievals for stratiform precipitation events observed at the SGP site to assess statistical variability and correlations between cloud and rainfall parameters, and in-depth analysis of the reasons for the higher LWP and $R_m$ retrieval noise when solving the full equation system (4) rather than using the simplified approach employed in this study. Future enhancements of the method could also include applying nonlinear W-band $\alpha_r$–$R$ relations and the use of the MMCR cirrus mode to improve ice retrievals near cloud tops.

*Acknowledgments.* This research was supported by the Office of Science (BER), U.S. Department of Energy, Grant DE-FG02-05ER63954. The author is thankful to Dr. Andrew J. Heymsfield for providing the dataset that was used for comparisons in Fig. 5 and to Dr. M. Shupe for help with extracting ARM measurement data.

## REFERENCES

Ackerman, T. P., and G. Stokes, 2003: The Atmospheric Radiation Measurement Program. *Phys. Today,* **56,** 38–45.

Barber, P., and C. Yeh, 1975: Scattering of electromagnetic waves by arbitrarily shaped dielectric bodies. *Appl. Opt.,* **14,** 2864–2872.

Bellon, A., G. W. Lee, and I. Zawadzki, 2005: Error statistics in VPR corrections in stratiform precipitation. *J. Appl. Meteor.,* **44,** 998–1015.

Brandes, E. A., G. Zhang, and J. Vivekanandan, 2005: Corrigendum. *J. Appl. Meteor.,* **44,** 186.

Comstock, J. M., and Coauthors, 2007: An intercomparison of microphysical retrieval algorithms for upper tropospheric ice clouds. *Bull. Amer. Meteor. Soc.,* **88,** 191–204.

Heymsfield, A. J., Z. Wang, and S. Y. Matrosov, 2005: Improved radar ice water content retrieval algorithms using coincident microphysical and radar measurements. *J. Appl. Meteor.,* **44,** 1391–1412.

Joss, J., and A. Waldvogel, 1967: Ein Spektrograph für Niederschlagstropfen mit automatisher Auswertung (A spectrograph for raindrop size measurement with automatic classification). *Pure Appl. Geophys.,* **68,** 240–246.

Kollias, P., and A. Albrecht, 2005: Why the melting layer radar reflectivity is not bright at 94 GHz. *Geophys. Res. Lett.,* **32,** L24818, doi:10.1029/2005GL024074.

——, E. E. Clothiaux, M. A. Miller, K. L. Johnson, K. P. Moran, K. B. Widener, and B. A. Albrecht, 2007: The Atmospheric Radiation Measurement Program cloud profiling radars: Second-generation sampling strategies, processing, and cloud data products. *J. Atmos. Oceanic Technol.,* **24,** 1199–1214.

Lhermitte, R., 2002: *Centimeter & Millimeter Wavelength Radars in Meteorology*. Lhermitte Publications, 550 pp.

Matrosov, S. Y., 2005: Attenuation-based estimates of rainfall rates aloft with vertically pointing $K_a$-band radars. *J. Atmos. Oceanic Technol.,* **22,** 43–54.

——, 2007: Potential for attenuation-based estimations of rainfall rate from CloudSat. *Geophys. Res. Lett.,* **34,** L05817, doi:10.1029/2006GL029161.

——, 2008: Assessment of radar signal attenuation caused by the melting hydrometeor layer. *IEEE Trans. Geosci. Remote Sens.,* **46,** 1039–1047.

——, and A. J. Heymsfield, 2008: Estimating ice content and extinction in precipitating cloud systems from CloudSat radar measurements. *J. Geophys. Res.,* **113,** D00A05, doi:10.1029/2007JD009633.

——, M. D. Shupe, A. J. Heymsfield, and P. Zuidema, 2003: Ice cloud optical thickness and extinction estimates from radar measurements. *J. Appl. Meteor.,* **42,** 1584–1597.

——, P. T. May, and M. D. Shupe, 2006: Rainfall profiling using atmospheric radiation measurement program vertically pointing 8-mm wavelength radars. *J. Atmos. Oceanic Technol.,* **23,** 1478–1491.

——, K. A. Clark, and D. E. Kingsmill, 2007: A polarimetric radar approach to identify rain, melting-layer, and snow regions for applying corrections to vertical profiles of reflectivity. *J. Appl. Meteor. Climatol.,* **46,** 154–166.

——, A. Battaglia, and P. Rodriguez, 2008a: Effects of multiple scattering on attenuation-based retrievals of stratiform rainfall from CloudSat. *J. Atmos. Oceanic Technol.,* **25,** 2199–2208.

——, M. D. Shupe, and I. V. Djalalova, 2008b: Snowfall retrievals using millimeter-wavelength cloud radars. *J. Appl. Meteor. Climatol.,* **47,** 769–777.

Mazin, I.P. 1989: *Clouds and the Cloudy Atmosphere* (in Russian). Gidrometeoizdat, 648 pp.

Miller, M. A., J. Verlinde, C. V. Gilbert, G. J. Lehenbauer, J. S. Tongue, and E. E. Clothiaux, 1998: Detection of nonprecipitating clouds with the WSR-88D: A theoretical and experimental survey of capabilities and limitations. *Wea. Forecasting,* **13,** 1046–1062.

Mosimann, L., 1995: An improved method for determining the degree of snow crystal riming by vertical Doppler radar. *J. Atmos. Res.,* **37,** 305–323.

Protat, A., J. Delanoe, D. Bouniol, A. J. Heymsfield, A. Bansemar, and P. Brown, 2007: Evaluation of ice water content retrievals from cloud radar reflectivity and temperature using a larger airborne in situ microphysical database. *J. Appl. Meteor. Climatol.,* **46,** 557–572.

Sheppard, B. E., and P. I. Joe, 1994: Comparisons of raindrop size distribution measurements by a Joss–Waldvogel disdrometer, a PMS 2DG spectrometer, and a POSS Doppler radar. *J. Atmos. Oceanic Technol.,* **11,** 874–887.

Stepanenko, V. D., G. G. Schukin, L. P. Bobylev, and S. Y. Matrosov, 1987: *Microwave Radiometry in Meteorology* (in Russian). Gidrometeoizdat, 284 pp.

Turner, D. D., and Coauthors, 2007: Thin liquid water clouds: Their importance and our challenge. *Bull. Amer. Meteor. Soc.,* **88,** 177–190.